Cellulose (2017) 24:69–84
DOI 10.1007/s10570-016-1101-0

ORIGINAL PAPER

Synthesis, characterization and properties of pineapple peel cellulose-*g*-acrylic acid hydrogel loaded with kaolin and sepia ink

Hongjie Dai · Huihua Huang

Received: 27 June 2016 / Accepted: 17 October 2016 / Published online: 1 November 2016

Abstract Novel composite hydrogels were synthesized by grafting of acrylic acid onto pineapple peel cellulose and addition of kaolin or sepia ink in ionic liquid 1-butyl-3-methylimidazolium chloride, using potassium persulfate as a free radical initiator and *N*,*N*′-methylenebisacrylamide as a crosslinking agent. The structure and morphology of the prepared hydrogels were characterized by Fourier transform infrared spectroscopy, field emission scanning electron microscope, X-ray diffraction, thermogravimetry and differential scanning calorimetry. Kaolin and sepia ink improved the thermal stability of the hydrogels. Swelling studies on the prepared hydrogels indicated sepia ink and kaolin affected the swelling ratio and pH-responsive properties. The optimum swelling pH value for the hydrogels was shifted from 7.0 to 12.0 in the presence of sepia ink. The effects of kaolin and sepia ink contents on methylene blue adsorption capacity of the prepared hydrogels were also investigated. The optimum methylene blue adsorption capacity reached 153.85 mg/g at 10% of kaolin and 142.21 mg/g at 20% of sepia ink. The pseudo-second-order kinetic model fit well with the experimental results, indicating the adsorption was chemisorption behavior.

Keywords Pineapple peel cellulose · Hydrogel · Acrylic acid · Kaolin · Sepia ink · Methylene blue

H. Dai · H. Huang (✉)
School of Food Science and Engineering, South China University of Technology, Guangzhou 510641, China
e-mail: fehhuang@scut.edu.cn

Present Address:
H. Huang
No. 381, Wushan Road, Tianhe District, Guangzhou City, Guangdong Province, China

Introduction

In recent years, many works have been devoted to studying the utilization of biomaterials, mainly the byproducts or wastes from industrial processing and agricultural waste materials. One of the most abundant biomaterials is pineapple (*Ananas comosus* L. Merryl) peel from the production of salads, juice, jam, canning and bromelain from pineapple (Da Silva et al. 2013; Nor et al. 2015; Wan et al. 2016). About 16–19 million tons of pineapple are produced around the world annually. Especially in can and juice processing, pineapple peel discharge produces waste of about 35% of the total pineapple weight and causes serious environmental issues (Hu et al. 2010). Hence, the multipurpose utilization of pineapple peel is of important significance. Pineapple peel is principally composed of cellulose, hemi-cellulose, lignin, pectin and so on, and cellulose generally accounts for 20–25% of the dry weight of the pineapple peel; however, only few studies have focused on the use of pineapple peel cellulose (Hu et al. 2013).

Cellulose is an extensive crystalline homo-polymer of anhydroglucopyranose units (AGU) via β-(1 → 4) glycosidic linkage and intra- and inter-molecular hydrogen bonds (Fengel and Wegener 1983). As the most abundant renewable resource on earth, cellulose has been translated into numerous new functional materials for a broad range of applications because of the increasing demand for "environmentally friendly" and biocompatible products in recent years (Zhang et al. 2015). Although cellulose is inexpensive, nontoxic, renewable, biodegradable, biocompatible and modifiable, its industrial applications are still limited because of its limited dissolution in water and common organic or inorganic solvents (Mai et al. 2016). Until now, only few solvent systems have been developed to effectively dissolve cellulose, such as *N*,*N*-dimethylacetamide/lithium chloride (DMAc/LiCl) (Zhang et al. 2014a, b), dimethyl sulfoxide/tetrabutylammonium fluoride (DMSO/TBAF) (Yusup et al. 2015), *N*,*N*-dimethylformamide/dinitrogen tetroxide (DMF/N_2O_4) (Mai et al. 2016), *N*-methylmorpholine-*N*-oxide (NMMO) (Jin et al. 2015) and NaOH/urea aqueous systems (Li et al. 2015). However, the main limitations in the practical use of these solvent systems are their toxicity, instability, high-cost, complex process and/or difficulties in reusability and recycling. Recently, room temperature ionic liquids (ILs) have been considered to be promising and green solvents for dissolving and processing cellulose owing to their low melting points, excellent dissolving capability, recyclability and negligible vapor pressure (Liu et al. 2015). For example, 1-allyl-3-methylimidazolium chloride (AmimCl), 1-butyl-3-methylimidazolium chloride (BmimCl) and 1-ethyl-3-methyl-imidazolium chloride (EmimCl) have been successfully used to process cellulose into composite materials for applications in the wastewater treatment, enzyme immobilization and drug delivery fields (Isik et al. 2014; Kim et al. 2012; Wang et al. 2013a, b; Xiong et al. 2014).

Hydrogels are three-dimensional networks of hydrophilic polymers formed by chemical and/or physical crosslinking and can absorb large quantities of water or biological fluids (Facin et al. 2015). Hydrogels with the characteristics responding to external stimulation such as temperature, pH, salt, light, electric fields and chemical environments are often referred to as "intelligent" or "smart" hydrogels, particularly those noncovalent dynamic bonding (hydrogen bonding, hydrophobic, π–π stacking and electrostatic interactions) dependent hydrogels (Chang et al. 2011). Compared with hydrogels prepared from synthetic polymers, hydrogels based on biopolymer such as cellulose, starch, chitosan, collagen and their derivatives have attracted great attentions recently due to their high hydrophilicity, biocompatibility, nontoxicity and biodegradability (Basri et al. 2016; Cheng et al. 2014; Facin et al. 2015; Kim et al. 2012; Peng et al. 2016). The cellulose-based smart hydrogels are particularly attractive because of the abundant source, high biocompatibility and excellent thermal and mechanical properties of cellulose. However, little literature about the utilization of pineapple peel cellulose has been reported so far, especially the preparation and application of pineapple peel cellulose-based hydrogels. Recently, our laboratory has reported that pineapple peel cellulose and the combinations with polyvinyl pyrrolidone (PVPP), polyethylene glycol (PEG), polyvinyl alcohol (PVA), r-carrageenan (CN) or soluble starch (SH) can be prepared in composite hydrogels by heating–cooling-washing or heating–cooling-freezing-thawing-washing processing in AmimCl (Hu et al. 2010, 2013). Moreover, our previous study reported that novel composite hydrogels based on pineapple peel cellulose and sepia ink were synthesized by homogeneous acetylation in BmimCl, and the composite hydrogels showed effective removal of methylene blue from aqueous solutions (Dai and Huang 2016). However, to our knowledge, there is no report about smart hydrogels prepared from pineapple peel cellulose.

Kaolin is a good adsorbent for removing contaminants from textile and dye industry wastewater and gradually is being used in preparing hydrogels because of its unique structure and high mechanical strength. (Pradhan et al. 2015; Shirsath et al. 2013). Sepia ink is mainly composed of melanin and shows obvious adsorption of Fe^{3+}, Cu^{2+}, Zn^{2+}, Cd^{2+}, Pb^{2+} and Ca^{2+}. However, until now, little literature has been available regarding the application of sepia ink in removing dye as well as in hydrogel preparation (Dai and Huang 2016). In this study, novel multi-component hydrogels were prepared by acrylic acid-grafting onto pineapple peel cellulose in the presence of kaolin and sepia ink; here, the graft of acrylic acid was to produce a pH-responsive characteristic for the hydrogels, and the incorporation of kaolin and sepia ink in hydrogels was

to improve the properties of the hydrogels such as the gel strength and mechanical, thermal stability and adsorption capacity. Based on the characterization by Fourier transform infrared spectroscopy (FTIR), scanning electron microscopy (SEM), X-ray diffraction (XRD), thermogravimetric analysis (TGA and DTG) and differential scanning calorimetry (DSC), the swelling behavior, pH sensitivity and methylene blue adsorption of the prepared hydrogels were investigated.

Materials and methods

Materials and reagents

Pineapple peel was obtained from a local pineapple processing factory (Guangzhou City, China). Ionic liquid 1-butyl-3-methylimidazolium chloride (BmimCl) was purchased from Lanzhou Institute of Chemistry Physics, Chinese Academy of Sciences (Lanzhou City, China). Kaolin was purchased from Tianjin Fuchen Chemical Reagent Co., Ltd. (Tianjin City, China). Acrylic acid (AA; purity ≥99.0%) was obtained from Tianjin Kermel Chemical Reagent Co., Ltd. (Tianjin City, China). Ammonium persulfate (APS; purity ≥98.0%) was supplied by Sinopharm Chemical Reagent Co., Ltd. (Shanghai City, China). *N*,*N*′-methylenebisacrylamide (MBA; purity ≥99.0%) was purchased from Tianjin Xinchun Chemical Reagent Co., Ltd. (Tianjin City, China). Methylene blue (MB; purity ≥98.5%) was supplied by Guangzhou Chemical Reagent Co., Ltd. (Guangzhou City, China). All other chemicals and solvents used in this experiment were of analytical grade.

Preparation of sepia ink

Cuttlefishes (*Sepia pharaonis*) were purchased from Xiashan Aquatic Products Wholesale Market (Zhanjiang City, China) in March 2015. After collection, identification and authentication by Round Beibu Gulf Institute for the Protection and Utilization of Marine Animals in Medicine, China, the cuttlefishes were immediately treated in the laboratory to obtain sepia ink. The ink sacs were removed from the cuttlefishes and washed with distilled water. After dissection, the ink was transferred into 800 ml distilled water in a 1000-ml beaker. The ink was immersed in distilled water overnight at room temperature to remove water-soluble impurities and then was centrifuged at $5000\times g$ for 20 min. The precipitate was collected and dried at 50 °C for 24 h. The dried ink was ground and passed through a 100-mesh sieve and then stored at −20 °C for further experiments.

Preparation of pineapple peel cellulose

Pineapple peel cellulose (PPC) was prepared by the method reported by Hu et al. (2010; 2013) with a few modifications. Pineapple peel was washed with distilled water to remove dirt and dried in an oven at 50 °C for 24 h. Thereafter, the dried peel was pulverized and sieved to a particle size of 150 to 200 μm. To extract the cellulose, the pineapple peel powder (50 g) was stir-treated with 1000 ml of distilled water at 80 °C for 2 h. The insoluble residue was collected and delignified with sodium chlorite solution (7.5%, w/v, pH 3.8–4.0, adjusted by 4 mol/l hydrochloric acid) at 75 °C for 2 h. After filtration, the residue was washed thoroughly with distilled water and ethanol (95%, v/v) three times by alternations and then was dried in an oven at 50 °C for 16 h. The dried residue was stir-treated with potassium hydroxide solution (10%, w/v) at room temperature for 10 h so as to remove the hemicellulose. Again after filtration, the residue was washed thoroughly with distilled water and 95% ethanol by turns until the filtrate was neutral. Finally, pineapple peel cellulose was available after drying in an oven at 50 °C for 16 h and pulverizing into a particle size of 150 to 200 μm. The yield of pineapple peel cellulose by the above processing was almost 23% (w/w).

Preparation of pineapple peel cellulose hydrogels

PPC (0.2 g) was mixed with 8 g of BmimCl and stir-treated at 90 °C for 5 h under N_2 atmosphere to guarantee complete dissolution. After cooling down to 60 °C, the calculated amount of initiator APS was added and kept at 60 °C for 15 min to generate radicals. Then, the mixture of AA (85% neutralization degree; adjusted by 40% sodium hydroxide solution at an ice bath) and MBA was added to the solution. The reaction was performed at 70 °C for 3 h under stirring and N_2 atmosphere. Then, the calculated kaolin (0–0.8 g) and sepia ink (0–0.12 g) were added into the mixture at 70 °C for 2 h under stirring to form a

homogeneous product. After the required time and cooling down to room temperature, the resulting mixture was slowly immersed in distilled water to remove the water-soluble oligomer, uncrosslinked polymer and unreacted monomer. Finally, the formed hydrogels were dried in a vacuum freeze drier at −50 °C for 36 h and stored at room temperature for further use. The detailed formulations for the hydrogels are listed in Table 1.

Characterization

Fourier transform infrared spectroscopy

Prior to measurement, the tested specimens were prepared by the KBr disk method. The FT-IR spectra of the samples were recorded on a FT-IR spectrometer (Vector 33, Bruker, Germany) from 400 to 4000 cm^{-1} at a resolution of 4 cm^{-1}.

Scanning electron micrograph

The internal surface morphology of the samples was observed using a field emission scanning electron microscope (S-3700N, Hitachi, Japan). Prior to observation, the surface of the samples was coated with a thin film of gold using a sputter coater (Cressington 108 auto, Watford, UK).

Table 1 Feed compositions of the hydrogels

Sample	PPC (g)	AA (g)	Kaolin (%)[a]	Sepia ink (%)[b]
PPCH-1[c]	0.2	0.8	0	20
PPCH-2	0.2	0.8	10	20
PPCH-3	0.2	0.8	25	20
PPCH-4	0.2	0.8	40	20
PPCH-5[d]	0.2	0.8	25	0
PPCH-6	0.2	0.8	25	40
PPCH-7	0.2	0.8	25	60
PPCH-8[e]	0.2	0.8	0	0

[a] Kaolin/PPC ratio by weight. For example, 10% (PPCH-2) indicates 0.02 g addition of the initial amount of kaolin

[b] Sepia ink/PPC ratio by weight. For example, 20% (PPCH-1) indicates 0.04 g addition of the initial amount of sepia ink

[c] Prepared without addition of kaolin (PPCH-1)

[d] Prepared without addition of sepia ink (PPCH-5)

[e] Prepared without addition of kaolin and sepia ink (PPCH-8)

X-ray diffraction

The XRD patterns of the samples were performed using an X-ray diffractometer (D8 ADVANCE, Bruker, Germany) with Cu-Ka radiation ($\lambda = 0.15418$ nm) as X-ray source at 40 kV of accelerating voltage and 40 mA of current. Scanning speed was set at 2°/min in the region of the diffraction angle (2θ) from 4° to 40° for the hydrogel samples and from 4° to 70° for sepia ink and kaolin.

Thermal analysis

Analysis of the thermal stability of the samples was performed based on thermal gravimetric analysis (TGA and DTG) and differential scanning calorimetry (DSC) using a simultaneous thermal analyzer (STA449C, NETZSCH, Germany) from the ambient temperature to 500 °C under N_2 atmosphere at 10 °C/min heating rate.

Study of properties

Swelling kinetics study

Prior to the swelling study, the hydrogels were cut and uniformed into small blocks of about 3 mm × 3 mm × 3 mm size. For swelling behavior analysis of the hydrogels, 25 mg of the prepared hydrogels was immersed into excessive distilled water at room temperature. After preset time intervals, the swollen hydrogels were removed from water and immediately weighed after blotting the excess water on the surface using filter paper. The swelling ratio (*SR*) was calculated according to the following equation:

$$\mathrm{SR}\ (\%) = \frac{W_t - W_d}{W_d} \times 100 \quad (1)$$

where W_d and W_t are the weights of the hydrogels before and after swelling at specified time intervals, respectively.

Evaluation of pH sensitivity

The gravimetric method was employed to measure the swelling ratio of the hydrogels in the aqueous solutions at different pH values from 2.0 to 12.0. The pH values were adjusted by HCl and NaOH solutions and determined by a pH meter (PHS-25, Shanghai Leici Instrument Co., Ltd., China). The ionic

strengths of all solutions were adjusted to 0.1 mol/l with NaCl solution. The uniformed hydrogels (25 mg) were immersed into excessive solutions at room temperature to reach swelling equilibrium. The swollen hydrogles were then removed from the solution and weighed immediately after eliminating the excess water on the surface using filter paper.

Adsorption of methylene blue

Adsorption experiments were carried out in a batch mode to study the effect of kaolin and sepia ink content on adsorption behavior. Prior to adsorption experiments, the hydrogels were cut into uniformed small blocks of about 3 mm × 3 mm × 3 mm. The uniformed hydrogel samples (25 mg) were immersed into 40 ml of MB aqueous solution of 100 mg/l at room temperature. After preset time intervals, the residual concentration of the MB solution was measured using a UV-vis spectrophotometer (UV-1800, Shimadzu, Japan) at 664 nm. The adsorption capacity of the hydrogels at time t (Q_t, mg/g), the equilibrium adsorption capacity (Q_e, mg/g) and the removal efficiency (R, %) of MB were calculated based on the following equation, respectively:

$$Q_t = \frac{(C_0 - C_t)V}{m} \quad (2)$$

$$Q_e = \frac{(C_0 - C_e)V}{m} \quad (3)$$

$$R = \frac{C_0 - C_e}{C_0} \times 100 \quad (4)$$

where C_0 and C_t (mg/l) are the concentrations of MB solution at the initial time and time t (h), respectively; C_e (mg/l) is the equilibrium concentration of the MB solution; V (L) is the volume of the MB solution, and m (g) is the weight of the dried hydrogels.

Results and discussion

Mechanism of hydrogel formation

In this research, hydrogels were prepared by crosslinking and grafting AA onto pineapple peel cellulose in the presence of kaolin and sepia ink. Generally, APS and MBA were used as a free radical initiator and a hydrophilic crosslinking agent, respectively. The proposed mechanism for grafting and chemically crosslinking reactions is outlined as Scheme 1. Initially, the persulfate initiator was decomposed into sulfate anion-radicals under heating and stirring. Subsequently, the sulfate anion-radicals extracted hydrogen from the hydroxyl group of PPC to form alkoxy radicals. Thus, the monomer molecule (AA) near to the vicinity of the reaction sites became acceptors of PPC radicals, resulting in chain initiation and thereafter conversion of itself into free radical donors at the neighboring molecules, and the grafted chain became extended. Then, the end vinyl groups of the crosslinker (MBA) reacted with the polymer chains during propagation of the chain to form a crosslinked structure. Here, kaolin may act as a crosslinking agent to form the network of the hydrogel, and sepia ink can be distributed on the surface or interior of the polymers. In order to minimize the damage effect of AA on kaolin and sepia ink structures, kaolin and sepia ink were added to the reaction mixture after 3 h. At this stage, the mixture had lower viscosity than the initial reaction mixture, which was beneficial for forming a uniformed mixture. In fact, the grafting and copolymerization reaction still continued until cooling down to room temperature and immersion into water. Therefore, kaolin and sepia ink could be effectively loaded in the network structure with this method, which is also confirmed by the subsequent SEM and XRD results in the present research. Bao et al. (2011) and Rashidzadeh et al. (2014) reported a basically identical reaction mechanism concerning the hydrogel prepared from sodium carboxymethyl cellulose-*g*-poly(acrylic acid-*co*-acrylamide-*co*-2-acrylamido-2-methyl-1-propanesulfonic)/montmorillonite and the hydrogel prepared from sodium alginate-*g*-poly(acrylic acid-*co*-acrylamide)/clinoptilolite hydrogel, respectively. Zhang et al. (2014a, b) also found a similar reaction mechanism for hydrogel prepared from maize bran-poly(acrylic acid).

Characterization

FT-IR spectra analysis

The FT-IR spectra of the initial substrates (PPC, sepia ink and kaolin) and the prepared hydrogels (PPCH-1, PPCH-5, PPCH-7 and PPCH-8) are depicted in Fig. 1. On the spectra of kaolin, the characteristic peaks at 1088 and 907 cm^{-1} can be considered as the attribute

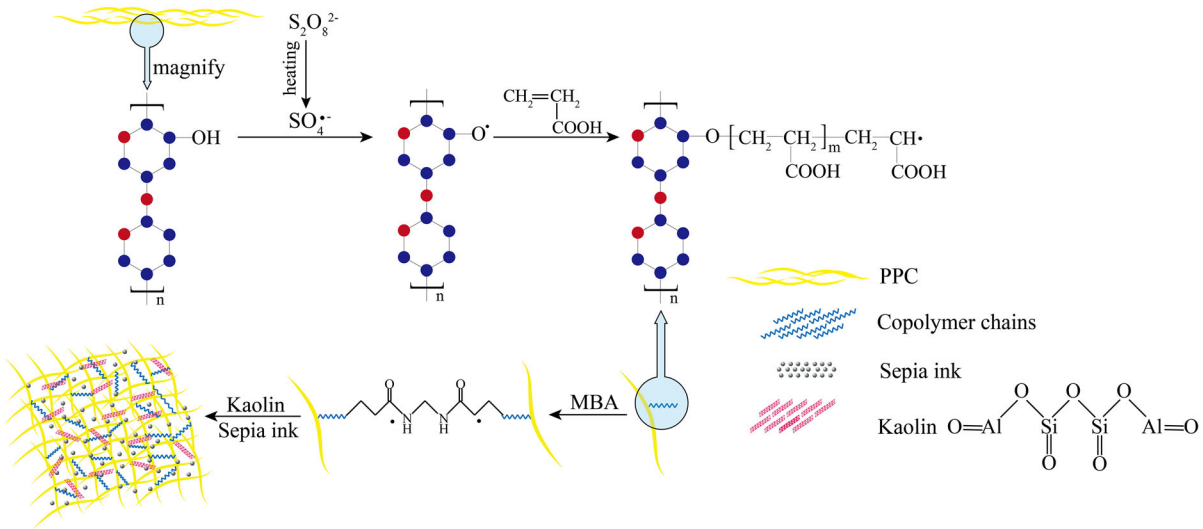

Scheme 1 Proposed reaction mechanism for the synthesis of PPC-*g*-AA/kaolin/sepia ink hydrogel

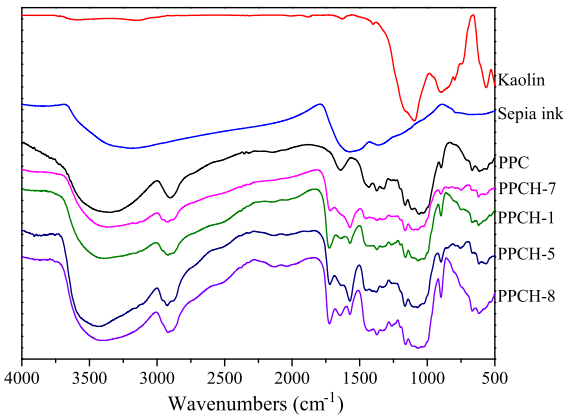

Fig. 1 FTIR spectra of kaolin, sepia ink, PPC and the prepared hydrogels PPCH-1, PPCH-5, PPCH-7 and PPCH-8

of the Si–O stretching vibration (Liu et al. 2010). The absorption peaks at 792 and 564 cm^{-1} can be assigned to the Si–O–Al stretching mode and Si–O–Al bending vibration, respectively (Bao et al. 2011). On the spectra of sepia ink, the absorption peaks at 3224, 1578 and 1368 cm^{-1} may be due to the O–H and N–H stretching vibrations, the ionization of COO– and C=O double bonds, and C–N stretching vibration, respectively, exhibiting the characteristic peaks of melanin (Guo et al. 2014; Moniruzzaman et al. 2015). On the spectra of PPC, the characteristic peaks at 3400, 2900, 1053 and 1436 cm^{-1} were ascribed to the stretching vibrations of O–H and N–H, C–H, C–O–C and the bending vibration of C–H, respectively, exhibiting the typical adsorption of native cellulose (Hu et al. 2010). Compared with the spectra of PPC, the hydrogels based on PPC showed some changes in their characteristic peaks; here, PPCH-1 and PPCH-7 prepared from PPC and sepia ink showed wider and flatter characteristic peaks at 3400 cm^{-1} because of O–H and N–H stretching vibrations, indicating the successful incorporation of sepia ink. PPCH-5 and PPCH-7 prepared from PPC and kaolin showed a weak peak at 565 and 559 cm^{-1} because of the Si–O–Al bending vibration, respectively, suggesting the successful grafting of kaolin. Furthermore, for all hydrogels, two newly appearing absorption peaks at 1567 and 1725 cm^{-1} were observed. The peak at 1567 cm^{-1} was assigned to the C=O asymmetric stretching from the carboxylate anion (Bao et al. 2011). The peak at 1725 cm^{-1} was attributed to the ester group formed during the graft reaction between AA and PPC. All these results indicate the successful grafting and synthesis of PPC-*g*-AA/kaolin/sepia ink hydrogels during the polymerization process.

SEM analysis

To determine the surface characteristics of the prepared hydrogels, SEM studies were performed. The SEM micrographs of PPCH-1, PPCH-5, PPCH-7, PPCH-8, PPC, sepia ink and kaolin are depicted in Fig. 2. As shown in Fig. 2a–c, as the initial substrates

of the prepared hydrogels, PPC (Fig. 2a) exhibited a significant rough structure of the fiber-like network. Sepia ink (Fig. 2b) and kaolin (Fig. 2c) consisted of small particles and few agglomerates. The diameters of sepia ink and kaolin particles were about 100–200 and 1–2 μm, respectively. Like the majority of freeze-dried hydrogels, the present hydrogels also depicted irregularly porous structures, as shown in Fig. 2d, e (top left). However, to study the effect of sepia ink and kaolin on the surface structure of the hydrogels, the SEM horizons were mainly focused on the relatively flat area of the hydrogels. As shown in Fig. 2d–f, after introducing kaolin and sepia ink, the SEM micrographs of PPCH-7, PPCH-1 and PPCH-5 showed that some small particles were well distributed on the surface of hydrogels, indicating the homogeneous insertion of sepia ink and kaolin into the graft copolymers. However, it was evident from Fig. 2g that PPCH-8 prepared without addition of sepia ink and kaolin exhibited a smooth surface instead of the fiber-like network structure of PPC and showed no particles. This may be attributed to the damage of the crystal structures of cellulose chains resulted from dissolution and modification (Zhang and Xia 2012).

XRD pattern analysis

The XRD patterns of the initial substrates (PPC, sepia ink and kaolin) and the prepared hydrogels are shown in Fig. 3. PPC exhibited a strong peak at $2\theta = 21.8°$ and two weak peaks at $2\theta = 15.3°$ and $2\theta = 34.6°$, corresponding to the typical diffraction peaks of the crystal structure of cellulose Iβ (Nam et al. 2016), while kaolin showed a strong crystalline peak at $2\theta = 20.2°$ and a broad peak at $2\theta = 26.3°$. The strong diffraction peaks of sepia ink at 2θ were around of 16.3°, 21.7°, 26.2° and 35.1°. Compared with the XRD pattern of PPC, there was only a decreased broad peak in intensity at around $2\theta = 20°–22°$ for PPCH-1 and PPCH-8, corresponding to the characteristic of amorphous cellulose (Nam et al. 2016; French 2014; French and Cintrón 2013). The XRD pattern differences among PPCH-1, PPCH-5, PPCH-7 and PPCH-8 may be due to the addition of kaolin. The peak at $2\theta = 26.2°$ only observed for PPCH-7 and PPCH-5 may be attributed to the incorporation of kaolin with a broad peak at $2\theta = 26.3°$. Meanwhile, it is considered that kaolin also can react with acrylic acid when grafting (Pourjavadi et al. 2008; Lungu et al. 2012).

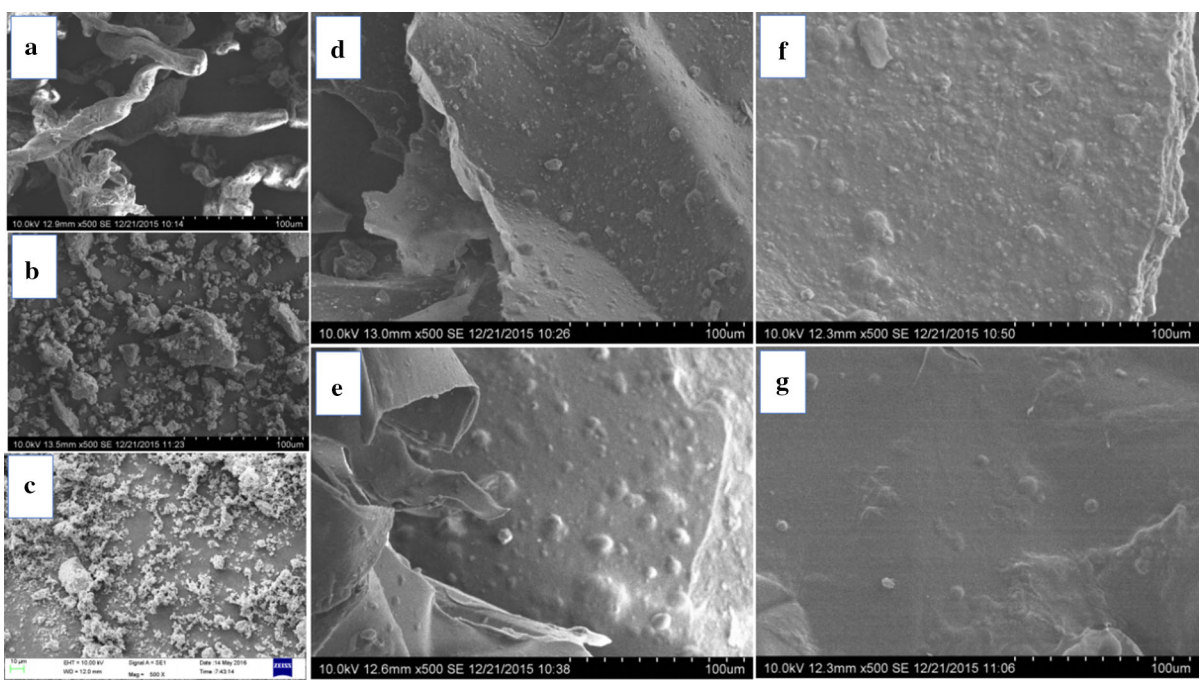

Fig. 2 SEM microgaraphs of PPC (**a**), sepia ink (**b**), kaolin (**c**), PPCH-7 (**d**), PPCH-1 (**e**), PPCH-5 (**f**) and PPCH-8 (**g**)

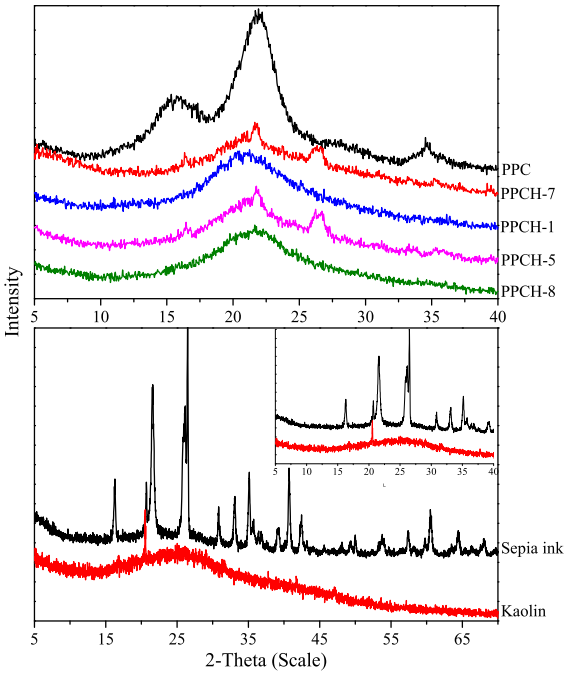

Fig. 3 XRD patterns of kaolin, sepia ink, PPC and the prepared hydrogels of PPCH-1, PPCH-5, PPCH-7 and PPCH-8

Hence, addition of kaolin would reduce the reaction between acrylic acid and PPC because of the competition of kaolin, finally resulting in the differences in XRD patterns among the different hydrogels. In addition, for PPCH-7, PPCH-1 and PPCH-5, the typical diffraction peaks of sepia ink or kaolin were found to have disappeared or been weakened, indicating that the sepia ink and kaolin inside the hydrogels were dispersed randomly in amorphous phase.

Thermal analysis

Considering the importance of thermal stability in applications of composite materials, the thermal properties of the initial substrates (PPC, sepia ink and kaolin) and the prepared hydrogels were studied and compared using a simultaneous thermal analyzer. The TGA and DTG curves for sepia ink, kaolin, PPC and the prepared hydrogels are depicted in Fig. 4. As shown in Fig. 4a, the TGA curve of sepia ink showed a continuous weight loss phase from 70 to 500 °C, and the TGA curve of kaolin was a horizontal line, indicating a better thermal stability. Compared with sepia ink and kaolin, the TGA curves of the PPC and the prepared hydrogels had an obvious weight loss that

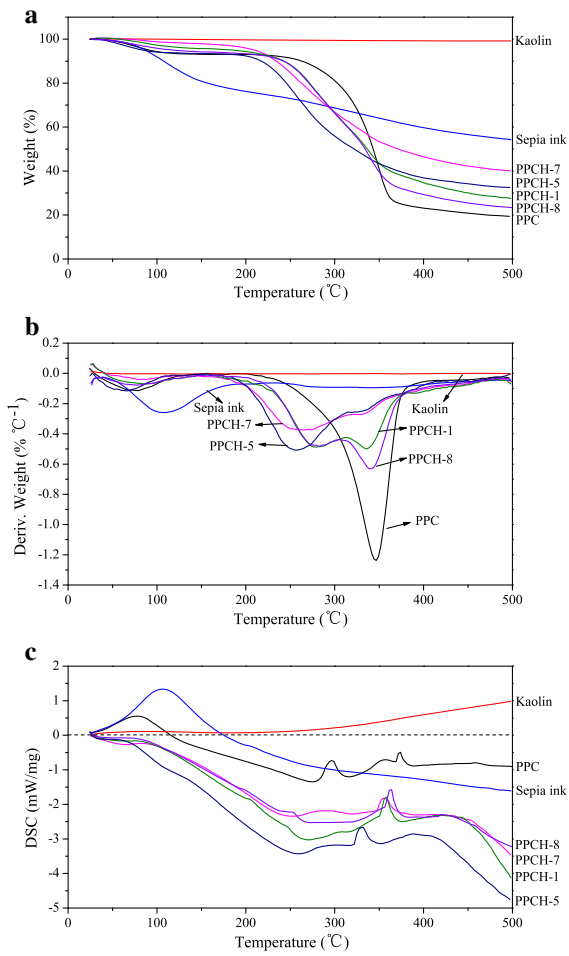

Fig. 4 TGA (**a**), DTG (**b**) and DSC (**c**) curves of kaolin, sepia ink, PPC and the prepared hydrogels PPCH-1, PPCH-5, PPCH-7 and PPCH-8

could be divided into two distinct stages from 25 to 500 °C. The first stage of weight loss appeared from 70 to 160 °C, corresponding to the loss of the adsorbed water or bound water in the samples. The second stage appeared from 190 to 400 °C, attributed to the thermal degradation of the base polymers, mainly resulted from the thermal decompositions of oxygen-containing functional groups such as carboxyl, hydroxyl, epoxy, nitrogen dioxide and ketone (Yadav et al. 2013; Zhuang et al. 2016). The initial decomposition temperature of PPC was 245 °C, significantly higher than that of the prepared hydrogels, suggesting that the prepared hydrogels had lower thermal stability than the native cellulose. Similar observations were also reported in other published works (Peng et al. 2014; Senna et al. 2014; Su et al. 2015). At above 500 °C, it

was found that PPC retained almost 20% of its initial mass, while PPCH-1, PPCH-5, PPCH-7 and PPCH-8 retained almost 28, 32, 40 and 23% (respectively) of the initial mass at the same temperature as above. However, kaolin and sepia ink retained almost 99 and 54%, respectively, of the initial mass at above 500 °C. The results demonstrated that the thermal stability of hydrogel was significantly increased because of the addition of sepia ink (PPCH-1), kaolin (PPCH-5) or the complex of sepia ink and kaolin (PPCH-7). This is in accordance with our previous study (Dai and Huang 2016). Pradhan et al. (2015) also found a high thermal stability for the nanohydrogel chitosan-*g*-PHEMA/kaolin because of the insertion of kaolin.

As shown in Fig. 4b, compared with PPC, the DTG curves of the hydrogels exhibited three main peaks from 25 to 500 °C. Besides the initial peak of the evaporation of water at around 75 °C and the last peak of cellulose degradation at around 350 °C, all the prepared hydrogels had a new peak at around 250–300 °C, with 260 °C for PPCH-5 and PPCH-7, and 280 °C for PPCH-1 and PPCH-8, respectively. Furthermore, as the hydrogels prepared without the addition of kaolin or sepia ink, PPCH-1 and PPCH-8 showed a slightly higher degradation rate at around 350 °C, indicating the beneficial effect of sepia ink and kaolin on improving the thermal stability of hydrogels.

The DSC curve reflecting the energy consumption characteristic during pyrolysis was also analyzed in this work. Figure 4c shows the DSC curves of kaolin, sepia ink, PPC and the prepared hydrogels. As shown in Fig. 4c, there was only one endothermic peak at around 108 °C for sepia ink, which was probably attributed to the degradation of polysaccharides or proteins in sepia ink (Derby 2014). For kaolin, there was no obvious endothermic peak at the preset temperature range, suggesting the better thermal stability of kaolin. For PPC, two sharp endothermic peaks were observed at around 296 and 374 °C, respectively, which was probably due to the degradation of cellulose and the destruction of the crystal structure. Compared with PPC, the prepared hydrogels including PPCH-1, PPCH-5, PPCH-7 and PPCH-8 showed only one sharp endothermic peak at 359, 330, 355 and 362 °C, respectively, which may be ascribed to the decomposition of cellulose inside hydrogels. However, at above 400 °C, the prepared hydrogels showed a broad and flat endothermic peak, indicating a higher temperature for decomposition of the prepared hydrogels.

Swelling studies

Swelling kinetics

Figure 5a shows the swelling kinetics of the prepared hydrogels of PPCH-1, PPCH-5, PPCH-7 and PPCH-8. Obviously, the prepared hydrogels exhibited a similar model of swelling kinetics. The swelling ratio increased sharply during the initial 40 min, reaching about 90% of the equilibrium value. The swelling ratio

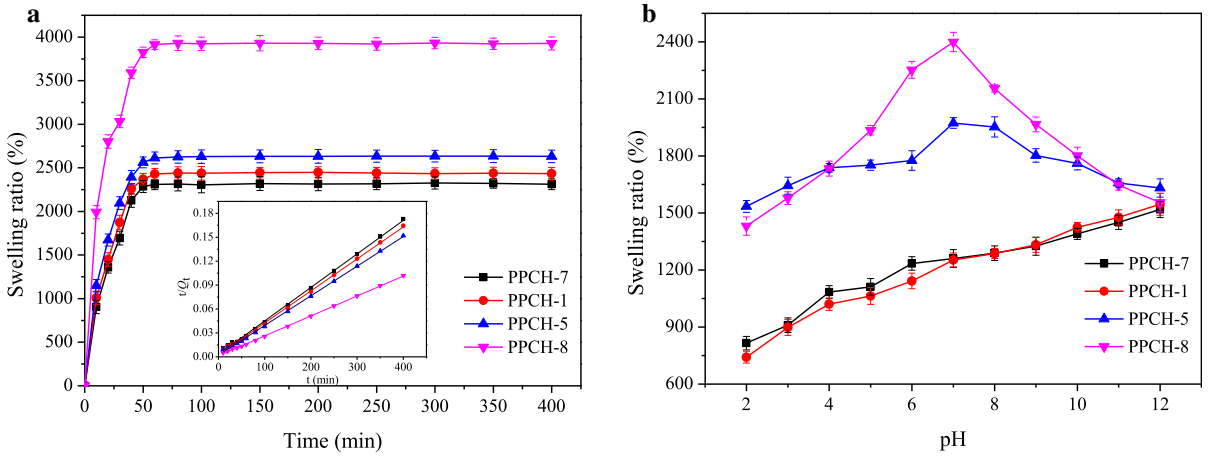

Fig. 5 Swelling kinetic curves (**a**) and pH sensitivities (**b**) of the prepared hydrogels PPCH-1, PPCH-5, PPCH-7 and PPCH-8 (sub-figure in **a** indicates the Schott's second-order kinetic model of the prepared hydrogels, and **b** indicates the effect of pH on the swelling ratio of the prepared hydrogels)

increased slowly after 40 min and almost reached a plateau after approximately 60 min. For evaluating the dynamic swelling properties of the prepared hydrogels, Schott's second-order kinetic model was applied and expressed in linear form as follows (Schott 1992):

$$\frac{t}{Q_t} = \frac{1}{kQ_e^2} + \frac{1}{Q_e}t \quad (5)$$

where Q_e (%) and Q_t (%) are the swelling ratios of the prepared hydrogels at equilibrium and any time (min), respectively. k (%/min) is the initial swelling rate constant. Based on the swelling data, the swelling kinetic parameters including the correlation coefficients (R^2), k and calculated swelling ratio ($Q_{e,cal}$) can be obtained by linear regression and displayed in Table 2. The plots of t/Q_t versus t displayed perfect straight lines with a good linear correlation coefficient ($R^2 > 0.99$; sub Fig. 5a), and the $Q_{e,cal}$ from the swelling kinetic model was very close to the experimental values ($Q_{e,exp}$), indicating that Schott's second-order kinetic model was suitable for evaluating the kinetic swelling behaviors of the prepared hydrogels. Compared with PPCH-8 without addition of sepia ink and kaolin, PPCH-1, PPCH-5 and PPCH-7 showed a higher initial swelling rate but lower equilibrium swelling ratio. On the one hand, the insertion of sepia ink and kaolin could increase the surface hydrophilicity of the hydrogels because of some functional groups in sepia ink and kaolin such as –COOH, –NH and –OH (Dai and Huang 2016; Pourjavadi et al. 2008); hence, the initial swelling rate of PPCH-1, PPCH-5 and PPCH-7 was increased. On the other hand, the insertion of sepia ink and kaolin also could lead to higher crosslinking density of the hydrogels (Pourjavadi et al. 2007), resulting in a lower equilibrium swelling ratio of PPCH-1, PPCH-5 and PPCH-7.

Table 2 Swelling kinetic parameters for the prepared hydrogels in distilled water at room temperature

Hydrogels	$Q_{e,exp}$ (%)	R^2	$Q_{e,cal}$ (%)	k (%/min)
PPCH-1	2433.2	0.9987	2493.3	6.4×10^{-5}
PPCH-5	2632.4	0.9991	2689.4	6.3×10^{-5}
PPCH-7	2312.8	0.9985	2378.4	5.9×10^{-5}
PPCH-8	3926.8	0.9994	3995.0	5.2×10^{-5}

pH sensitivity of the prepared hydrogels

The swelling ratio of the prepared hydrogels (PPCH-1, PPCH-5, PPCH-7 and PPCH-8) was investigated in the aqueous solutions at different pH values from 2.0 to 12.0. As observed in Fig. 5b, the swelling behaviors of the prepared hydrogels clearly exhibited pH sensitivity. For PPCH-5 and PPCH-8, the swelling ratio considerably increased with the increased pH from 2.0 to 7.0 and then significantly decreased within pH 7.0–12.0. The maximum swelling ratio was observed at pH 7.0. However, for PPCH-7 and PPCH-1, the swelling ratio continuously increased with the increased pH values from 2.0 to 12.0. The obvious pH-dependent change of the prepared hydrogels in the swelling ratio demonstrated the excellent pH-sensitive characteristic. This intriguing pH-dependent behavior of the prepared hydrogels could be attributed to the following reasons. The prepared hydrogels contained numerous hydrophilic $–COO^-$ and –COOH groups in their network structures that could convert with each other. Under acid medium (usually at pH <4), most of the $–COO^-$ groups were protonated from $–COO^-$ to –COOH; subsequently, the hydrogen-bonding interaction among –COOH groups was strengthened, and an additional physical crosslinking was generated. In the meantime, the electrostatic repulsion among $–COO^-$ groups was restricted; thus, the diffusion of water into the network structure of the prepared hydrogels was impaired, finally resulting in a low swelling ratio at low pH values (Peng et al. 2011). On the contrary, as the external pH increased, the opposite process occurred, and the swelling ratio increased. The reason was that the hydrogen-bonding interactions were broken beccause of the ionization of –COOH groups from –COOH to $–COO^-$. Besides, the reinforcement of the electrostatic repulsion between $–COO^-$ groups also caused an increased swelling ratio. However, under alkaline conditions, the charge screening effect of Na^+ counterions in the swelling medium could prevent effective anion–anion repulsions and subsequently led to decreased swelling ratio (Zhou et al. 2013). For these reasons, PPCH-5 and PPCH-8 showed a decrease of the swelling ratio at high pH values. However, the swelling ratio of PPCH-1 and PPCH-7 exhibited a continuous increase at high pH values. This may be attributed to the increase of $–COO^-$ groups in hydrogels because of the addition of sepia ink, subsequently leading to an increase of

electrostatic repulsion among the $-COO^-$ groups accompanied by the increased swelling ratio.

MB adsorption kinetics analysis and comparison between the prepared hydrogels

As adsorption kinetics can be used to describe the dye adsorption rate and eventually to explore the mechanism and possible rate-controlling steps of adsorption, in this study, a series of MB adsorption experiments were carried out to investigate the effect of contents of kaolin and sepia ink in the prepared hydrogels on MB adsorption capacity (Q_t). The results are shown in Fig. 6. It can be clearly seen that the Q_t of MB increased rapidly during the initial adsorption phase (prior to the 37th h) and then showed a further slow increase over the time, and it finally reached absorption equilibrium after approximately 120 h. This is attributed to a higher initial MB concentration and abundant free adsorption sites available during the initial adsorption phase (Fu et al. 2015). Figure 6a, c shows the effect of the kaolin content on the adsorption capacities of the prepared hydrogels for MB. As shown in Fig. 6a, the adsorption capacity first increased and then decreased as the kaolin content increased. For the hydrogels of PPCH-1, PPCH-2, PPCH-3 and PPCH-4, their kaolin contents were 0, 10, 25 and 40%, respectively. Compared with PPCH-1 and PPCH-4, PPCH-2 and PPCH-3 showed a higher adsorption capacity for MB. After the initial adsorption phase, the Q_t values of PPCH-1, PPCH-2, PPCH-3 and PPCH-4 were 119.95, 140.63, 142.21, and 111.32 mg/g, respectively. As shown in Fig. 6c, at adsorption equilibrium, the Q_t values of PPCH-1, PPCH-2, PPCH-3 and PPCH-4 were 144.86, 153.85, 151.59 and 148.99 mg/g, respectively, and the removal efficiency of MB reached 88.81, 95.45, 93.78 and 91.86%, respectively, indicating the appropriate kaolin content was 10%. At low kaolin content, kaolin was easily ionized and dispersed into the hydrogels, thus enhancing the hydrophilicity of the hydrogels, which was advantageous for adsorption behavior. However, an overly high increase of kaolin content in the hydrogels led to high crosslinking density and filled up the polymeric network of the hydrogels with kaolin physically, which was harmful to the adsorption of MB (Shi et al. 2013; Zhu et al. 2014).

Figure 6b, d depicts the effect of sepia ink content on the adsorption capacities of the prepared hydrogels for MB. It can be seen that the sepia ink content is an important factor affecting the MB adsorption capacity of the prepared hydrogels. For hydrogels PPCH-5, PPCH-3, PPCH-6 and PPCH-7, their sepia ink contents were 0, 20, 40 and 60%, respectively. As shown in Fig. 6b, after the initial adsorption phase, the Q_t values of PPCH-5, PPCH-3, PPCH-6 and PPCH-7 were 122.70, 142.21, 128.94 and 107.22 mg/g, respectively; however, at absorption equilibrium, the Q_t values of PPCH-5, PPCH-3, PPCH-6 and PPCH-7 reached 146.73, 151.59, 145.55 and 149.04 mg/g, respectively, and the removal efficiency of MB reached 90.19, 93.78, 89.32 and 92.26%, respectively, as shown in Fig. 6d, suggesting the adequate content of sepia ink in hydrogels was 20%. Our previous study also confirmed the positive effect of sepia ink on MB adsorption of PPC hydrogels because of the functional groups in sepia ink including COO–, N–H and O–H (Dai and Huang 2016). However, similar to kaolin, the sepia ink also exhibited an opposite effect on MB adsorption at high content in the hydrogels. This phenomenon may be attributed to the excessive accumulation of sepia ink on the surface or inside of the prepared hydrogels, resulting in a low swelling ratio and high crosslinking density (Pourjavadi et al. 2007).

The pseudo-first-order kinetic and the pseudo-second-order kinetic models were most commonly used to investigate the rate constant and analyze the mechanism of the adsorption process. These two kinetic models can be expressed in linear form as follows (Dai and Huang 2016):

$$\mathrm{Log}\,(Q_e - Q_t) = \mathrm{Log}\,Q_e - \frac{k_1 t}{2.303} \tag{6}$$

$$\frac{t}{Q_t} = \frac{1}{k_2 Q_e^2} + \frac{1}{Q_e} t \tag{7}$$

where Q_e (mg/g) and Q_t (mg/g) are the MB adsorption capacities of the prepared hydrogels at equilibrium and any time (h), respectively. k_1 (h^{-1}) and k_2 (mg/g h^{-1}) are the rate constants of the pseudo-first-order kinetic and pseudo-second-order kinetic models, respectively. The fitted curves of the pseudo-first-order and pseudo-second-order kinetic models are shown in the sub figures of Fig. 6a, b. The kinetic parameters including correlation coefficients (R^2), k_1,

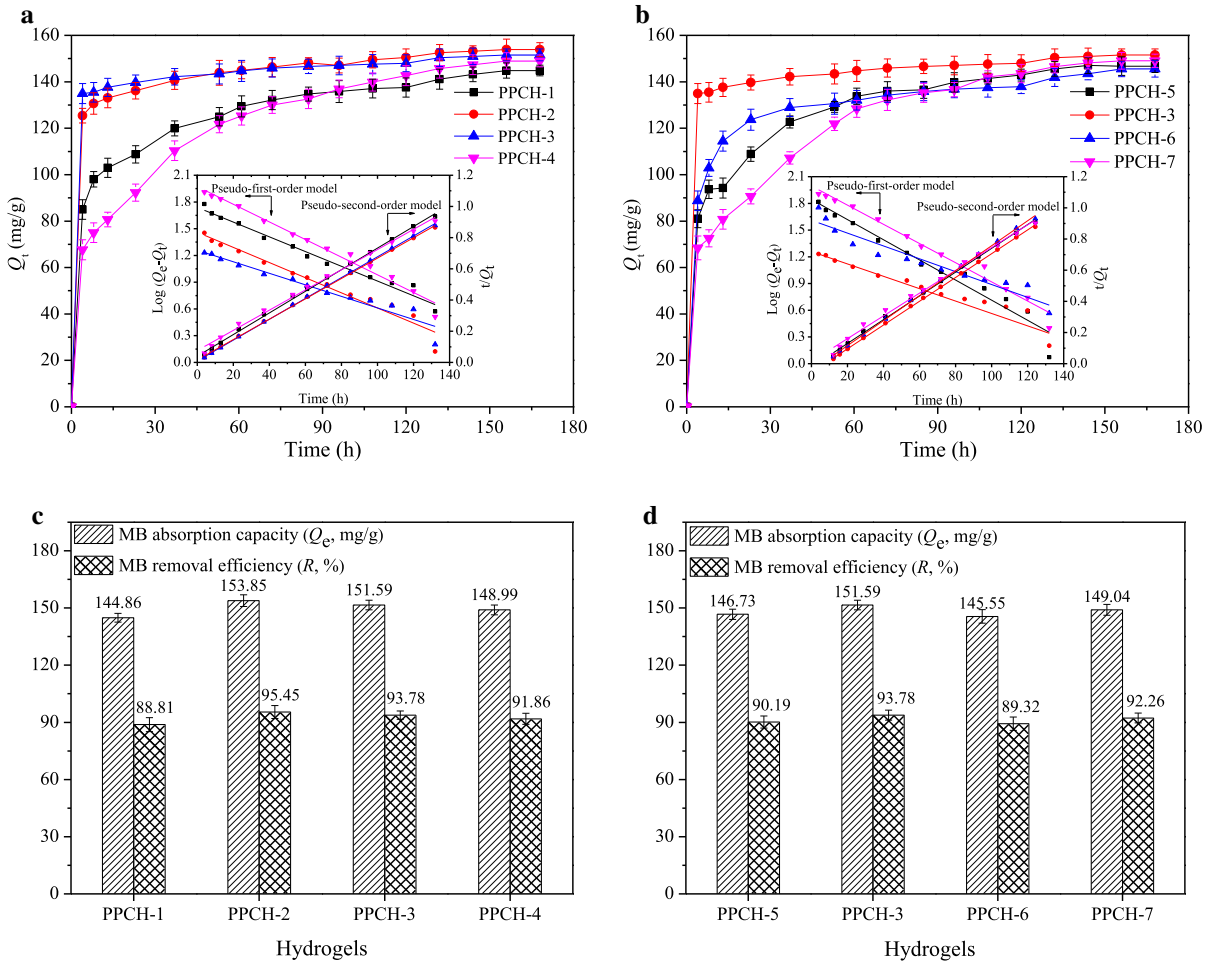

Fig. 6 Effect of kaolin content (**a**, **c**) and sepia ink content (**b**, **d**) of hydrogels on MB adsorption kinetic curves, equilibrium adsorption capacity and removal efficiency (sub figures in **a** and **b** indicate the comparison of pseudo-first-order kinetic and pseudo-second-order kinetic models of MB adsorption and the *arrows* in the figures specify the *left* or *right* *y*-axis that the curve follows)

k_2 and calculated Q_e values ($Q_{e,cal}$) can be obtained by linear regression based on the experimental data, as shown in Table 3. For all the prepared hydrogels, the R^2 obtained from the pseudo-second-order kinetic model was larger than 0.99, indicating a good fit of the model with the experimental data sets. In addition, the $Q_{e,cal}$ from the pseudo-first-order kinetic model failed to predicate the experimental equilibrium amount of absorbed MB ($Q_{e,exp}$), while the $Q_{e,cal}$ from the pseudo-second-order kinetic model agreed well with the $Q_{e,exp}$, further suggesting that the adsorption process followed the pseudo-second-order model rather than pseudo-first-order model and the MB adsorption of the prepared hydrogels was controlled by the chemisorption behavior, including the likely ion exchange and π–π stacking interaction between cation groups of the dye and functional groups (mainly –COOH, –NH and –OH) of the biomass surface (Chen et al. 2015; Dai and Huang 2016). Figure 7 depicts the color change of the hydrogel and MB solution after the completion of adsorption and describes the MB adsorption behaviors of the prepared hydrogels. The adsorption capacity of the prepared hydrogels for MB was compared with the other reported natural polymer-based adsorbents listed in Table 4. It could be concluded that the prepared hydrogels possessed a higher MB adsorption capacity (153.85 mg/g) than other reported

Table 3 Kinetic parameters of the pseudo-first-order kinetic and pseudo-second-order kinetic models for MB adsorption of the prepared hydrogels

Hydrogels	$Q_{e,exp}$ (mg/g)	Pseudo-first-order kinetic			Pseudo-second-order kinetic		
		R^2	$Q_{e,cal}$ (mg/g)	k_1 (h^{-1})	R^2	$Q_{e,cal}$ (mg/g)	k_2 (mg/g h^{-1})
PPCH-1	144.86	0.9777	54.93	0.0190	0.9983	144.30	4.80×10^{-5}
PPCH-2	153.85	0.9546	28.87	0.0196	0.9994	153.14	4.26×10^{-5}
PPCH-3	151.59	0.9303	18.14	0.0149	0.9996	149.93	4.45×10^{-5}
PPCH-4	148.99	0.9811	94.68	0.0228	0.9945	154.56	4.19×10^{-5}
PPCH-5	146.73	0.9550	69.74	0.0260	0.9983	149.93	4.45×10^{-5}
PPCH-6	145.55	0.9148	40.81	0.0166	0.9992	142.65	4.91×10^{-5}
PPCH-7	149.04	0.9771	99.03	0.0248	0.9938	156.50	4.08×10^{-5}

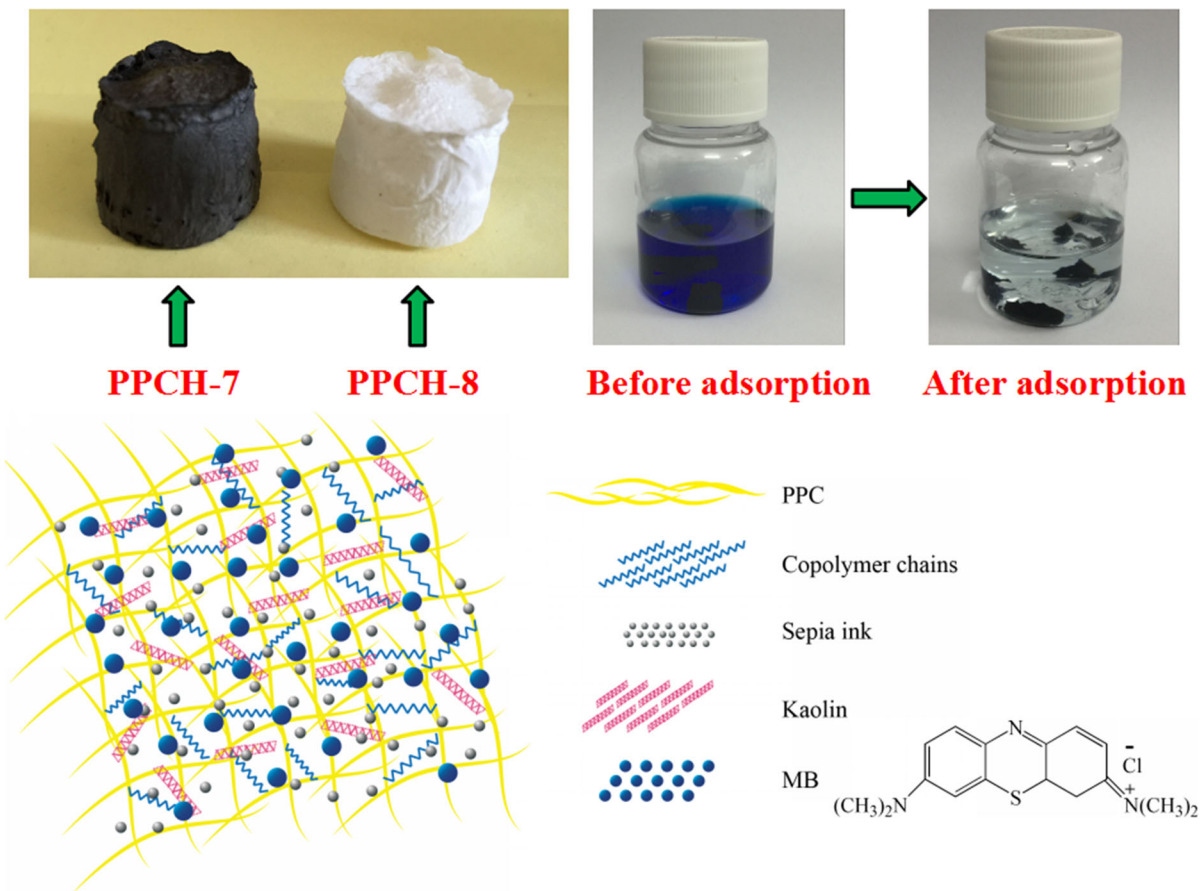

Fig. 7 Changes in color of the hydrogels prepared with and without the addition of sepia ink (PPCH-7 and PPCH-8, respectively) and MB solution after the completion of adsorption and the scheme to describe the MB adsorption behavior of the prepared hydrogels

natural-polymer-based adsorbents. Hence, the prepared hydrogels are potential efficient adsorbents for removal of MB with environmentally friendly and economically cost-effective merits.

Conclusion

Novel composite hydrogels were prepared by grafting acrylic acid onto pineapple peel cellulose and

Table 4 Comparison of the adsorption capacities between the prepared hydrogels and other natural polymer-based adsorbents for MB

Natural polymer-based adsorbents	Maximum adsorption capacity (mg/g)	References
Starch-humic acid composite hydrogel beads	110	Chen et al. (2015)
Unmodified cellulose	50	Yan et al. (2011)
Carboxymethyl-β-cyclodextrin/Fe_3O_4 nanoparticles	140.8	Badruddoza et al. (2010)
β-Cyclodextrin polymer crosslinked by citric acid	105	Zhao et al. (2009)
Modified gum arabic hydrogels	48	Paulino et al. (2006)
Cellulose/poly(*N*-isopropylacrylamide) hydrogels	2.8	Wang et al. (2013a, b)
Magnetic chitosan/graphene oxide composites	132.6	Fan et al. (2012)
Alginate-graft-poly(methyl methacrylate) beads	5.25	Salisu et al. (2015)
Magnetic carboxymethyl starch/poly(vinyl alcohol) composite gel	23.53	Gong et al. (2015)
Modified pineapple peel cellulose hydrogels embedded with sepia ink[a]	138.25	Dai and Huang (2016)
Pineapple peel cellulose-*g*-acrylic acid/kaolin/sepia ink hydrogels[b]	153.85	This work

[a] Reported in our previous studies (Dai and Huang 2016)

[b] PPCH-2, containing 10% kaolin and 20% sepia ink

additions of kaolin or sepia ink. Successful grafting of acrylic acid was confirmed by FTIR. The homogeneous insertion of kaolin and sepia ink was also confirmed by SEM and XRD. The results of TGA, DTG and DSC analysis showed sepia ink and kaolin had a positive effect on improving the thermal stability of the prepared hydrogels. Swelling studies of the prepared hydrogels indicated that sepia ink and kaolin affected the swelling ratio and the pH-responsive characteristic. The MB adsorption capacity of the hydrogels was influenced by the contents of kaolin and sepia ink. The pseudo-second-order kinetic model fit well with the experimental results, indicating the adsorption was a chemisorption behavior.

Acknowledgements This work was supported by the National Natural Science Foundation of China under Grant Nos. 31471673 and 31271978 and the Ministry of Education PRC under Grant No. 20120172110017.

References

Badruddoza A, Hazel GSS, Hidajat K, Uddin MS (2010) Synthesis of carboxymethyl-β-cyclodextrin conjugated magnetic nano-adsorbent for removal of methylene blue. Colloid Surf A 367:85–95. doi:10.1016/j.colsurfa.2010.06.018

Bao Y, Ma J, Li N (2011) Synthesis and swelling behaviors of sodium carboxymethyl cellulose-*g*-poly(AA-*co*-AM-*co*-AMPS)/MMT superabsorbent hydrogel. Carbohydr Polym 84:76–82. doi:10.1016/j.carbpol.2010.10.061

Basri SN, Zainuddin N, Hashim K, Yusof NA (2016) Preparation and characterization of irradiated carboxymethyl sago starch-acid hydrogel and its application as metal scavenger in aqueous solution. Carbohydr Polym 138:34–40. doi:10.1016/j.carbpol.2015.11.028

Chang C, He M, Zhou J, Zhang L (2011) Swelling behaviors of pH-and salt-responsive cellulose-based hydrogels. Macromolecules 44:1642–1648. doi:10.1021/ma102801f

Chen R, Zhang Y, Shen L, Wang X, Chen J, Ma A, Jiang W (2015) Lead(II) and methylene blue removal using a fully biodegradable hydrogel based on starch immobilized humic acid. Chem Eng J 268:348–355. doi:10.1016/j.cej.2015.01.081

Cheng Y, Lu J, Liu S, Zhao P, Lu G, Chen J (2014) The preparation, characterization and evaluation of regenerated cellulose/collagen composite hydrogel films. Carbohydr Polym 107:57–64. doi:10.1016/j.carbpol.2014.02.034

Da Silva DIS, Nogueira GDR, Duzzioni AG, Barrozo MAS (2013) Changes of antioxidant constituents in pineapple (*Ananas comosus*) residue during drying process. Ind Crop Prod 50:557–562. doi:10.1016/j.indcrop.2013.08.001

Dai HJ, Huang H (2016) Modified pineapple peel cellulose hydrogels embedded with sepia ink for effective removal of methylene blue. Carbohydr Polym 148:1–10. doi:10.1016/j.carbpol.2016.04.040

Derby CD (2014) Cephalopod ink: production, chemistry, functions and applications. Mar Drugs 12:2700–2730. doi:10.3390/md12052700

Facin BR, Moret B, Baretta D, Belfiore LA, Paulino AT (2015) Immobilization and controlled release of β-galactosidase from chitosan-grafted hydrogels. Food Chem 179:44–51. doi:10.1016/j.foodchem.2015.01.088

Fan L, Luo C, Sun M, Li X, Lu F, Qiu H (2012) Preparation of novel magnetic chitosan/graphene oxide composite as effective adsorbents toward methylene blue. Bioresour Technol 114:703–706. doi:10.1016/j.biortech.2012.02.067

Fengel D, Wegener G (1983) Wood: chemistry, ultrastructure, reactions. Walter de Gruyter, Berlin

French AD (2014) Idealized powder diffraction patterns for cellulose polymorphs. Cellulose 21:885–896. doi:10.1007/s10570-013-0030-4

French AD, Cintrón MS (2013) Cellulose polymorphy, crystallite size, and the Segal crystallinity index. Cellulose 20:583–588. doi:10.1007/s10570-012-9833-y

Fu J, Chen Z, Wang M, Liu S, Zhang J, Zhang J, Han R, Xu Q (2015) Adsorption of methylene blue by a high-efficiency adsorbent (polydopamine microspheres): kinetics, isotherm, thermodynamics and mechanism analysis. Chem Eng J 259:53–61. doi:10.1016/j.cej.2014.07.101

Gong G, Zhang F, Cheng Z, Zhou L (2015) Facile fabrication of magnetic carboxymethyl starch/poly(vinyl alcohol) composite gel for methylene blue removal. Int J Biol Macromol 81:205–211. doi:10.1016/j.ijbiomac.2015.07.061

Guo X, Chen S, Hu Y, Li G, Liao N, Ye X, Liu D, Xue C (2014) Preparation of water-soluble melanin from squid ink using ultrasound-assisted degradation and its anti-oxidant activity. J Food Sci Technol 51:3680–3690. doi:10.1007/s13197-013-0937-7

Hu X, Hu K, Zeng L, Zhao M, Huang H (2010) Hydrogels prepared from pineapple peel cellulose using ionic liquid and their characterization and primary sodium salicylate release study. Carbohydr Polym 82:62–68. doi:10.1016/j.carbpol.2010.04.023

Hu X, Wang J, Huang H (2013) Impacts of some macromolecules on the characteristics of hydrogels prepared from pineapple peel cellulose using ionic liquid. Cellulose 20:2923–2933. doi:10.1007/s10570-013-0075-4

Isik M, Sardon H, Mecerreyes D (2014) Ionic liquids and cellulose: dissolution, chemical modification and preparation of new cellulosic materials. Int J Mol Sci 15:11922–11940. doi:10.3390/ijms150711922

Jin X, Liu X, Liu Q, Li Y (2015) Manufacture and performance of ethylamine hydroxyethyl chitosan/cellulose fiber in *N*-methylmorpholine-*N*-oxide system. React Funct Polym 91–92:62–70. doi:10.1016/j.reactfunctpolym.2015.04.008

Kim MH, An S, Won K, Kim HJ, Lee SH (2012) Entrapment of enzymes into cellulose–biopolymer composite hydrogel beads using biocompatible ionic liquid. J Mol Catal B Enzym 75:68–72. doi:10.1016/j.molcatb.2011.11.011

Li R, Wang S, Lu A, Zhang L (2015) Dissolution of cellulose from different sources in an NaOH/urea aqueous system at low temperature. Cellulose 22:339–349. doi:10.1007/s10570-014-0542-6

Liu Y, Wang W, Wang A (2010) Adsorption of lead ions from aqueous solution by using carboxymethyl cellulose-*g*-poly(acrylic acid)/attapulgite hydrogel composites. Desalination 259:258–264. doi:10.1016/j.desal.2010.03.039

Liu Z, Sun X, Hao M, Huang C, Xue Z, Mu T (2015) Preparation and characterization of regenerated cellulose from ionic liquid using different methods. Carbohydr Polym 117:99–105. doi:10.1016/j.carbpol.2014.09.053

Lungu A, Perrin FX, Belec L, Sarbu A, Teodorescu M (2012) Kaolin/poly(acrylic acid) composites as precursors for porous kaolin ceramics. Appl Clay Sci 62:63–69. doi:10.1016/j.clay.2012.04.008

Mai NL, Kim CK, Park B, Park H, Lee SH, Koo Y (2016) Prediction of cellulose dissolution in ionic liquids using molecular descriptors based QSAR model. J Mol Liq 215:541–548. doi:10.1016/j.molliq.2016.01.040

Moniruzzaman M, Ono T, Bustam MA, Yusup S, Uemura Y (2015) Pretreatment of wood biomass with ionic liquids: a "green" approach to separate cellulose for use in oilfield application. J Appl Sci 15:531–537. doi:10.3923/jas.2015.531.537

Nam S, French AD, Condon BD, Concha M (2016) Segal crystallinity index revisited by the simulation of X-ray diffraction patterns of cotton cellulose Iβ and cellulose II. Carbohydr Polym 135:1–9. doi:10.1016/j.carbpol.2015.08.035

Nor MZM, Ramchandran L, Duke M, Vasiljevic T (2015) Characteristic properties of crude pineapple waste extract for bromelain purification by membrane processing. J Food Sci Technol 52:7103–7112. doi:10.1007/s13197-015-1812-5

Paulino AT, Guilherme MR, Reis AV, Campese GM, Muniz EC, Nozaki J (2006) Removal of methylene blue dye from an aqueous media using superabsorbent hydrogel supported on modified polysaccharide. J Colloid Interface Sci 301:55–62. doi:10.1016/j.jcis.2006.04.036

Peng X, Ren J, Zhong L, Peng F, Sun R (2011) Xylan-rich hemicelluloses-graft-acrylic acid ionic hydrogels with rapid responses to pH, salt, and organic solvents. J Agr Food Chem 59:8208–8215. doi:10.1021/jf201589y

Peng S, Meng H, Ouyang Y, Chang J (2014) Nanoporous magnetic cellulose–chitosan composite microspheres: preparation, characterization, and application for Cu(II) adsorption. Ind Eng Chem Res 53:2106–2113. doi:10.1021/ie402855t

Peng N, Wang Y, Ye Q, Liang L, An Y, Li Q, Chang C (2016) Biocompatible cellulose-based superabsorbent hydrogels with antimicrobial activity. Carbohydr Polym 137:59–64. doi:10.1016/j.carbpol.2015.10.057

Pourjavadi A, Hosseinzadeh H, Sadeghi M (2007) Synthesis, characterization and swelling behavior of gelatin-*g*-poly(-sodium acrylate)/kaolin superabsorbent hydrogel composites. J Compos Mater 41:2057–2069. doi:10.1177/0021998307074125

Pourjavadi A, Ayyari M, Amini-Fazl MS (2008) Taguchi optimized synthesis of collagen-*g*-poly(acrylic acid)/kaolin composite superabsorbent hydrogel. Eur Polym J 44:1209–1216. doi:10.1016/j.eurpolymj.2008.01.032

Pradhan AK, Rana PK, Sahoo PK (2015) Biodegradability and swelling capacity of kaolin based chitosan-*g*-PHEMA nanocomposite hydrogel. Int J Biol Macromol 74:620–626. doi:10.1016/j.ijbiomac.2014.12.024

Rashidzadeh A, Olad A, Salari D, Reyhanitabar A (2014) On the preparation and swelling properties of hydrogel nanocomposite based on sodium alginate-*g*-poly(acrylic acid-*co*-acrylamide)/clinoptilolite and its application as slow release fertilizer. J Polym Res 21:1–15. doi:10.1007/s10965-013-0344-9

Salisu A, Sanagi MM, Karim KJA, Pourmand N, Ibrahim WAW (2015) Adsorption of methylene blue on alginate-grafted-poly(methyl methacrylate). Jurnal Teknologi 76:19–25

Schott H (1992) Swelling kinetics of polymers. J Macromol Sci B 31:1–9. doi:10.1080/00222349208215453

Senna AM, Novack KM, Botaro VR (2014) Synthesis and characterization of hydrogels from cellulose acetate by

esterification crosslinking with EDTA dianhydride. Carbohydr Polym 114:260–268. doi:10.1016/j.carbpol.2014.08.017

Shi Y, Xue Z, Wang X, Wang L, Wang A (2013) Removal of methylene blue from aqueous solution by sorption on lignocellulose-*g*-poly(acrylic acid)/montmorillonite three-dimensional cross-linked polymeric network hydrogels. Polym Bull 70:1163–1179. doi:10.1007/s00289-012-0898-4

Shirsath SR, Patil AP, Patil R, Naik JB, Gogate PR, Sonawane SH (2013) Removal of brilliant green from wastewater using conventional and ultrasonically prepared poly(acrylic acid) hydrogel loaded with kaolin clay: a comparative study. Ultrason Sonochem 20:914–923. doi:10.1016/j.ultsonch.2012.11.010

Su Y, Liu J, Yue Q, Li Q, Gao B (2015) Adsorption of lead and nickel ions by semi-interpenetrating network hydrogel based on wheat straw cellulose: kinetics, equilibrium, and thermodynamics. Soft Mater 13:225–236. doi:10.1080/1539445X.2015.1074923

Wan J, Guo J, Miao Z, Guo X (2016) Reverse micellar extraction of bromelain from pineapple peel—effect of surfactant structure. Food Chem 197:450–456. doi:10.1016/j.foodchem.2015.10.145

Wang J, Wei L, Ma Y, Li K, Li M, Yu Y, Wang L, Qiu H (2013a) Collagen/cellulose hydrogel beads reconstituted from ionic liquid solution for Cu(II) adsorption. Carbohydr Polym 98:736–743. doi:10.1016/j.carbpol.2013.06.001

Wang J, Zhou X, Xiao H (2013b) Structure and properties of cellulose/poly(*N*-isopropylacrylamide) hydrogels prepared by SIPN strategy. Carbohydr Polym 94:749–754. doi:10.1016/j.carbpol.2013.01.036

Xiong R, Wang Y, Zhang X, Lu C (2014) Facile synthesis of magnetic nanocomposites of cellulose@ ultrasmall iron oxide nanoparticles for water treatment. RSC Adv 4:22632–22641. doi:10.1039/C4RA01397B

Yadav M, Rhee KY, Jung IH, Park SJ (2013) Eco-friendly synthesis, characterization and properties of a sodium carboxymethyl cellulose/graphene oxide nanocomposite film. Cellulose 20:687–698. doi:10.1007/s10570-012-9855-5

Yan H, Zhang W, Kan X, Dong L, Jiang Z, Li H, Yang H, Cheng R (2011) Sorption of methylene blue by carboxymethyl cellulose and reuse process in a secondary sorption. Colloid Surf A 380:143–151. doi:10.1016/j.colsurfa.2011.02.045

Yusup EM, Mahzan S, Jafferi N, Been CW (2015) The effectiveness of TBAF/DMSO in dissolving oil palm empty fruit bunch-cellulose phosphate. J Med Bioeng 4:165–169

Zhang YD, Xia XZ (2012) Physicochemical Characteristics of pineapple (*Ananas* mill.) peel cellulose prepared by different methods. Adv Mater Res 554–556:1038–1041. doi:10.4028/www.scientific.net/AMR.554-556.1038

Zhang C, Liu R, Xiang J, Kang H, Liu Z, Huang Y (2014a) Dissolution mechanism of cellulose in *N*,*N*-dimethylacetamide/lithium chloride: revisiting through molecular interactions. J Phys Chem 118:9507–9514. doi:10.1021/jp506013c

Zhang M, Cheng Z, Zhao T, Liu M, Hu M, Li J (2014b) Synthesis, characterization, and swelling behaviors of salt-sensitive maize bran–poly(acrylic acid) superabsorbent hydrogel. J Agric Food Chem 62:8867–8874. doi:10.1021/jf5021279

Zhang W, Sha Z, Huang Y, Bai Y, Xi N, Zhang Y (2015) Glow discharge electrolysis plasma induced synthesis of cellulose-based ionic hydrogels and their multiple response behaviors. RSC Adv 5:6505–6511. doi:10.1039/C4RA11222A

Zhao D, Zhao L, Zhu C, Huang W, Hu J (2009) Water-insoluble β-cyclodextrin polymer crosslinked by citric acid: synthesis and adsorption properties toward phenol and methylene blue. J Incl Phenom Macro 63:195–201. doi:10.1007/s10847-008-9507-4

Zhou Y, Fu S, Zhang L, Zhan H (2013) Superabsorbent nanocomposite hydrogels made of carboxylated cellulose nanofibrils and CMC-*g*-p(AA-*co*-AM). Carbohydr Polym 97:429–435. doi:10.1016/j.carbpol.2013.04.088

Zhu L, Zhang L, Tang Y, Kou X (2014) Synthesis of sodium alginate graft poly(acrylic acid-*co*-2-acrylamido-2-methyl-1-propane sulfonic acid)/attapulgite hydrogel composite and the study of its adsorption. Polym Plast Technol 53:74–79. doi:10.1080/03602559.2013.843691

Zhuang Y, Yu F, Chen J, Ma J (2016) Batch and column adsorption of methylene blue by graphene/alginate nanocomposite: comparison of single-network and double-network hydrogels. J Environ Chem Eng 4:147–156. doi:10.1016/j.jece.2015.11.014